Automatic Ship Detection on Multispectral and Thermal Infrared Aerial Images Using MACS-Mar Remote Sensing Platform

Jörg Brauchle, Steven Bayer, Ralf Berger

German Aerospace Center (DLR), Institute of Optical Sensor Systems
Berlin, Germany
{Joerg.Brauchle | Steven.Bayer | Ralf.Berger}@DLR.de

Abstract: The Modular Aerial Camera System (MACS) is a development platform for optical remote sensing concepts, algorithms and special environments. For Real-Time Services for Maritime Security (EMSec joint project) a new multi-sensor configuration MACS-Mar was realized. It consists of 4 co-aligned sensor heads in the visible RGB, near infrared (NIR, 700-950 nm), hyperspectral (HS, 450-900 nm) and thermal infrared (TIR, 7.5…14 µm) spectral range, a mid-cost GNSS/INS system, a processing unit and two data links. On-board image projection, cropping of redundant data and compression enable the instant generation of direct-georeferenced high resolution image mosaics, automatic object detection, vectorization and annotation of floating objects on the water surface. The results were transmitted over a distance up to 50 km in real-time via narrow and broadband data links and were visualized in a maritime situation awareness system.

For the automatic onboard detection of objects a segmentation and classification workflow based on RGB, NIR and TIR information was developed and tested in September 2016. The completeness of the object detection in the experiment resulted in 95 %, the correctness in 53 %. Mostly bright backwash of ships led to overdetection of the number of objects, further refinement using water homogeneity in the TIR, as implemented in the workflow, couldn't be carried out due to problems with the TIR sensor. To analyze the influence of high resolution TIR imagery and to reach the expected detection quality a further experiment was conducted in August 2017. Adding TIR images the completeness was increased to 98 % and the correctness to 74 %.

Keywords : maritime security; ship detection; MACS; real-time; aerial camera

1 Introduction

Remote sensing methods have been used in maritime scenarios for many years with different scopes that can be attributed to maritime security and safety [1]. Passive optical sensors in multi-spectral or hyper-spectral configurations are widely used for the monitoring of large-scale ecological issues like algal blooms, coral reef studies, or the analysis of sediment transport in estuaries [2][3]. The inclusion of thermal infrared allows for additional applications like monitoring thermal plumes of warm water discharges caused by power plants [4][5]. With the constant improvement of spatial resolution, also ship detection is now possible from satellite based passive optical systems [6][7]. Radar and especially synthetic aperture radar (SAR) have been studied for sea state monitoring [8][9], oil spill [10] and ship detection [11][12], especially exploiting the benefits of a satellite platform regarding the vast area of interest. Also satellite based receivers for 'Automatic Identification System' (AIS) are under study and in experimental use [13][14].

All those sensors and methods have been tested or applied also on airborne platforms [14]. Especially security related applications benefit from the feasible higher spatial resolutions, combinations of sensors [16] and the merging with information from ground-based sensors or sensor networks [17]. Therefore an extensive suite of instruments and methods is available for gathering information about the maritime environment.

Several of these remotes sensing methods are applied today in a regular manner. German Navy operates a pollution control aircraft mainly for oil spill detection [18], several national search-and-rescue operations use helicopters equipped with multi-sensor reconnaissance payloads [19]. Also, in Germany the main agencies with maritime security tasks have created a joint 'Maritime Safety and Security Center of the Federal Government and the Coastal States' in which information gathered by the contributing partners are shared [20].

Nonetheless, remote sensing is only scarcely and sporadically applied for maritime security challenges. Patrolling extended areas with a plane or assigning singular missions to sensor-equipped helicopters does not amount to constant, multi-scale situation awareness. Relatively high effort is necessary to sustain the aforementioned solutions especially given the comparatively low risk of incidents. This is a limiting factor for the establishment of persistent and comprehensive maritime monitoring system. Also ship- and ground-based installations like AIS and Radar are often seen to be generally adequate.

Information in maritime environment is shared predominantly by direct voice communication between stakeholders. A unified view on the situation for every participant is all but impossible. With a rising number from about 1,300 marine incidents and casualties reported to the European Maritime Security Agency in 2011 to about 3,300 in 2016 [21], a combination of diverse methods to enable a robust maritime situation awareness over an extended time-frame is deemed necessary at least for regions of particular interest.

Our objective in the joint project ‚Echtzeitdienste für die Maritime Sicherheit – EMSec' ('Real-Time Services for Maritime Security – EMSec') was the development of a special airborne camera system including processing and data deployment, which had to meet several user-defined requirements. The main products were to deliver a high-resolution true-color overview of a confined area (georeferenced image mosaic) as well as automatically detected and annotated objects on the water surface. Every product had to be provided in real-time to an existing ground-based central situation awareness system and its human-machine-interface.

2 Methodology

2.1 Automatic Object Detection

One goal of the experiment is the detection of small floating objects in water. For a generally applicable method it is very important to develop universal algorithms which are working in different environments, recording times and under changing weather and water conditions; that is a big challenge.

Besides extraction algorithms input data has a big influence on extraction results. In order to have a functional algorithm it is necessary to use the special characteristics of each sensor. One useful sensor for object detection in a maritime environment is a thermal IR imager. Because of almost homogeneous water temperature and the missing effect of sun glint a thermal image is suitable to detect objects of a certain minimum size on water with a very high accuracy. Due to the ground sampling distance (GSD) of thermal IR images (1.22 m GSD at 2,500 m altitude) small objects like sea marks or persons in water cannot be extracted reliably. Common RGB and NIR sensors can provide sufficient resolution. At an altitude for our surveillance flights of 2,500 m the used RGB sensor has a GSD of 0.37 m and the NIR sensor of 0.49 m (Table 2).

For the development of the algorithm a flight altitude of 2,500 m was assumed. So in our case the thermal IR images are used for the detection of objects with a size of more than 1.5 m x 2.5 m. Offshore most objects have a larger size than 1.5 m x 2.5 m. Therefore by using thermal IR images a bulk of objects can be detected. However, the existence of smaller objects cannot be excluded. Due to this reason the RGB and NIR images are additionally necessary to improve the completeness of object extraction. On the one hand the main advantage of RGB and NIR images is the higher GSD in comparison to the thermal IR images. On the other hand maritime RGB and NIR images are mainly influenced by sun glint [22]. Sun glint is the specular reflection of sunlight from water surface into the sensor [23]. This is an enormous source of irritation and leads to incorrect object detections. For successful object detection the effect of sun glint has to be reduced significantly.

In order to discover water pollution NIR and hyperspectral sensors are helpful. An overview of airborne sensors for water quality assessment is given in a review [24]. The proposed method to detect water quality [25] was developed by the team Optical Remote Sensing of Water at the DLR.

Based on the specific characteristics of all but hyperspectral sensors an automatic object detection algorithm in maritime environments was developed. The algorithm is divided into five parts (Fig. 1).

I. Preprocessing to identify regions of interest and the reduction of sun glint in RGB and NIR images as well as noise in thermal IR images.
II. Image segmentation.
III. Classification and object detection.
IV. Improvement of object border (reshaping).
V. Object catagorization (object catalog).

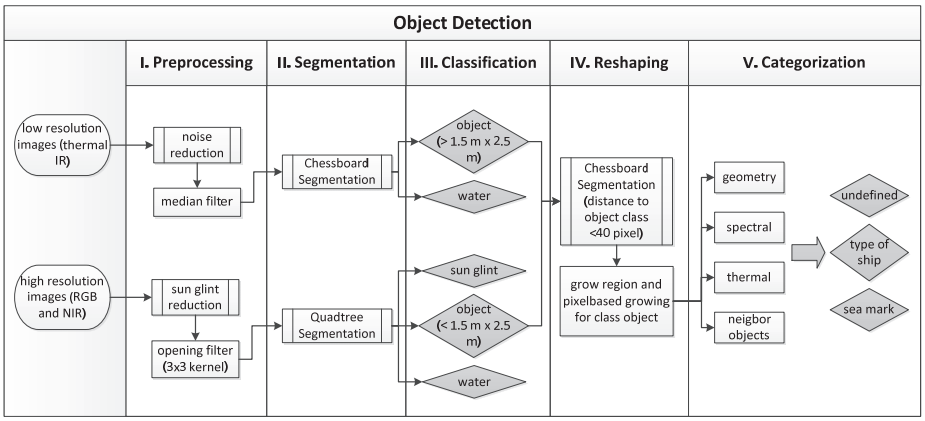

Fig. 1. Object detection algorithm flow chart

Test flights with the DLR-developed aerial camera MACS (chapter 3.1) showed that sun glint has a negative influence on automatic object detection. Due to the reflection and refraction of sun light on waves many incorrect objects were detected. Because of this effect a very fast preprocessing of the images became necessary. Because of the realtime preprocessing on the camera system the complex existing algorithms for sun glint reduction were not suitable. Therefore we used a software-based opening filter [26]. to reduce the impact of sun glint (Fig. 2). The opening filter was used with a 3x3 kernel. By using this kernel all objects were preserved and the sun glint was reduced partly but not completely. A 5x5 kernel reduced the sun glint but very small objects as well. As Fig. 2b shows the used 3x3 opening filter can not remove the whole sun glint. Because of that fact sun glint still had an influence on object extraction results.

The thermal IR images have a small noise. Therefore a median filter was used to reduce the noise.

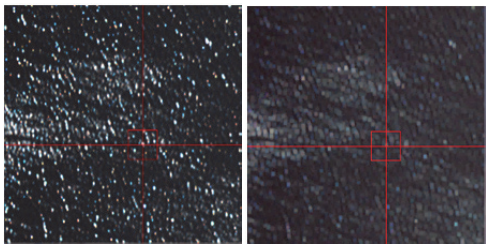

a) b)

Fig. 2. Reduce of sun glint; a) RGB image, b) image after opening filter

The filtered aerial images were used for image segmentation (part II). For high resolution images a quadtree segmentation (Fig. 3a) was implemented due to almost homogeneous water surface and short processing time. Chessboard segmentation was used for the thermal IR images which are more homogeneous and have a lower resolution.

Based on the segments a very simple and transferable local thresholding classification algorithm was executed to distinguish between water, sun glint and objects within high resolution images. For every channel the mean of the whole image was calculated (image mean) and added with a value of 8,000 which was determined empirically. This value depends on light conditions and was changeable by operator during the flight. The classification is based on comparing image mean with the mean of the segments. For the object class the blue and the red channels were used. If the mean of the segment in the blue or red channel was less than image mean the segment was classified as an object. Following the object segments were merged. For sun glint classification it was assumed that the brightness of sun glint segment is higher than a water segment and that sun glint affects only small areas. If the image mean was less than the segment mean of the red, green, blue and NIR channel as well as the segment was smaller than 2 m² the segment was classified as sun glint. The other segments were classified as water (part III).

To distinguish between water and objects within low resolution thermal IR images in part III a standard deviation was calculated. Therefore the 49 neighbour pixels of each pixel (three rows around center) were considered to find pixels with high contrast. It was assumed that water has homogeneous temperature and objects on the water have clear temperature difference. If the standard deviation was more than 0.5 the pixel was classified as an object pixel. All object pixels were merged to filled polygons. Small objects of less than 1.5 m x 2.5 m were removed.

In part IV the border of detected objects was improved applying a region- and pixel based growing algorithm. This step was necessary for the following object identification.

Object identification was implemented in the final (part V) step to distinguish between different ship types (red objects), sea marks (small green object) and undefined objects (Fig. 3d). Therefore geometric (size and shape) and spectral properties as well as relations to neighbour objects were used. For example, a ship is an elongated object which is longer than wide and surrounded by water. The type of ship was distinguished by size (Table 1).

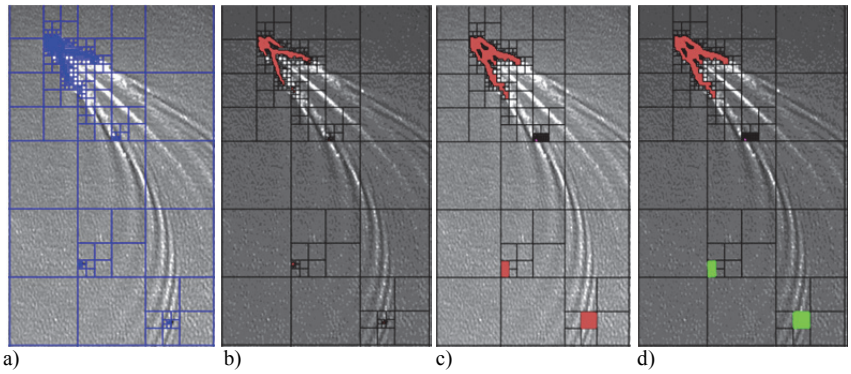

Fig. 3. Steps of automatic object detection with a) segmentation, b) classification, c) border improvement, d) object identification

Table 1. Ship size categories

Type of ship	Size [m x m]
Yacht	< 20 x 5
Ferry / small cargo ship	< 150 x 25
Container ship / huge cargo ship	> 400 x 60

2.2 Accuracy Assessment

An accuracy analysis is executed to evaluate the automatic object detection accuracy. Due to the fact that outlines of an object cannot be extracted exactly in many cases the evaluation of the accuracy for every object is a challenge. The automatically extracted objects may be too small, too big or just a sub-part of another extracted object. Hence for every object it is necessary to decide whether extraction is correct or false. According to Egenhofer [27] eight theoretical relations between two objects are possible, divided into correct, false, and unclear cases. In the latter cases it has to be distinguished between correct and false extracted objects. This can be estimated by the overlapping factor [28]:

$$OF = \frac{|\ \mathcal{A}^\circ \cap \mathcal{B}^\circ\ |}{min(|\ \mathcal{A}^\circ\ |\ ,\ |\ \mathcal{B}^\circ\ |)} \tag{1}$$

with OF = overlapping factor
A° = extent of object A
B° = extent of object B.

The object is extracted as false if the overlapping factor in our case is equal or smaller than 0.3. This value was determined empirically during previous campaigns. An object is correctly extracted if the overlapping factor is greater than 0.3. The determination as false, correct and missed objects is executed with the overlapping factor. During the EMSec test campaigns which are described in chapters 3.2 and 3.3,

all recorded objects were identified and automatic object detection algorithm was applied to aerial imagery. After the identification of correct, false and missed objects the determination of the overall accuracy is possible. To determine the accuracy the completeness (producers accuracy) and the correctness (users accuracy) according to Straub [29] is calculated. The completeness (com) of the results is calculated as:

$$\text{com}\ (\%) = \frac{\text{ceo}}{\text{ceo} + \text{neo}} * 100 \tag{2}$$

The correctness (corr) of the results is calculated as:

$$\text{corr}\ (\%) = \frac{\text{ceo}}{\text{ceo} + \text{weo}} * 100 \tag{3}$$

with ceo = correctly extracted objects, neo = not extracted objects, weo = wrong extracted objects.

3 Experiment

3.1 MACS – Modular Aerial Camera System

The MACS camera system enables the fast and easy development of novel aerial camera concepts for special applications [30][31]. Multiple passive optical sensors can be combined to acquire the relevant information (Fig. 4). The sensors and their field of vision can be adjusted to specific use-cases. All sensors and their optics are calibrated geometrically and for radiometric correction. The mechanical design must be rigid to allow for a precise co-registration of images taken by all sensors of the respective configuration. To efficiently evaluate such a configuration, an approach for combined photogrammetric processing of multiple sensor heads had been developed [32].

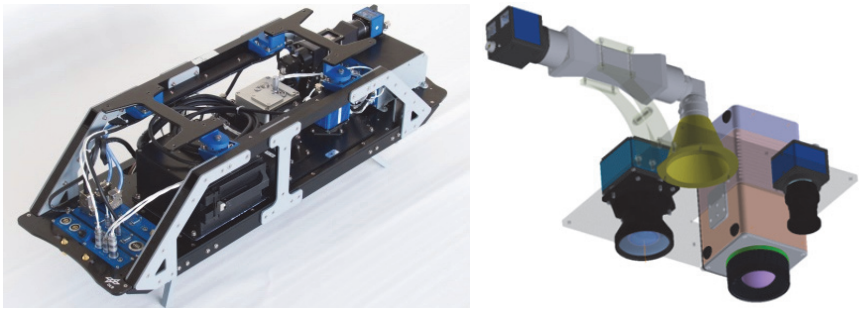

Fig. 4. MACS-Mar configuration with RGB, NIR, thermal IR, hyperspectral

Image processing and recording is done by a desktop class embedded computer. This computational power is necessary to allow for simultaneous recording of various sensor data, online georeferencing, map projection of those data and implementation of suitable real-time image classification algorithms. In this way, various higher level geoinformation can be generated automatically during operation. The automatic ob-

jects of interest detection is based on co-registered image map and executed in real-time. As any pixel of the maps created has a reliable coordinate and time designation, the same applies to any detected object. By sending only detected objects to a ground station, the amount of data to be transmitted can be reduced and the amount of information to be examined by an human operator decreases.

The sensor system is controlled via ground-based mission control center through a 9,600 Bit per second narrowband radio link. The operator is able to monitor system healthiness, to change the configuration and to receive classification results. The current position of the aircraft and the footprints of the images taken are shown continuously on a scalable moving map. Enabling a more powerful air-to-ground link providing a data rate of 5 – 10 Megabit per second, seamless cropped images are transmitted in full geometric and radiometric resolution (Fig. 5).

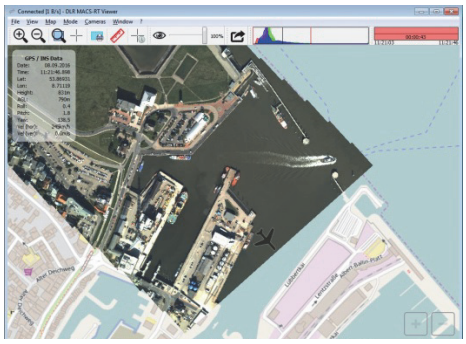

Fig. 5. Real-time map with full geometric and radiometric resolution

The visual information can be directly interpreted by humans. In addition, object detection algorithms are applicable. Different sensors and lenses can be used which allow task-specific footprints and ground resolutions. A ground sampling distance of up to 3 cm is achievable depending on the flight altitude and optical configuration. Within the map, distances and areas can be determined, e.g. the length of a vessel or the extent of oil contamination areas.

3.2 Joint EMSec experiment

During a verification experiment, stretching over several days, a set of scenarios was carried out. One scenario simulated the hijacking of a ferry ship and subsequent deactivation of AIS for a covert change of the course [33]. MACS-Mar was used to deliver information about objects on the water surface and to deliver detailed optical imagery for interpretation assistance for human operators.

Carried by the autopilot-controlled DLR research aircraft Dornier 228 (D-CODE) [34], MACS-Mar operated largely automatically. Data products were delivered continuously via radio link. All geo-referencing, mosaicking and image interpretation tasks were designed to operate on board automatically, so the derived information could be directly put into distribution system and human-machine interface.

To match the specific requirements of the EMSec project and following the investigation of preliminary work [35], four optical sensor heads acquiring wavelengths from 400 nm to 14 µm were chosen (Table 2). Fig. 4 shows the MACS-Mar remote sensing system including both narrowband and broadband data links.

From 5th to 9th September 2016 the EMSec experiment was conducted over the North Sea off Cuxhaven. Different sub-experiments were performed with more than 9 hours of image acquisition including dusk operation at solar altitude down to 2.5 degree.

Table 2. MACS-Mar Sensor Set-up

	RGB (Bayer color pattern)	**Near Infrared**	**Thermal Infrared**	**Hyperspectral**
Spectral Bands (nm)	400 – 520 (blue) 500 – 590 (green) 590 – 680 (red)	700-950	7,500 – 14,000	450 – 950 (105 channels)
Resolution (pixels)	4,864 x 3,232	3,296 x 2,472	1,024 x 768	80 x 80
GSD @ 820 m above sea level (cm)	12	16	40	400
GSD @ 2,500 m above sea level (cm)	37	49	122	1220
Field of view across track (deg)	40	36	32	22

3.3 Thermal imagery experiment

During the joint EMSec experiment unfortunately the thermal IR sensor did not work properly. Insufficient amount of data was acquired to perform the intended object detection analysis. In August 2017 a second experiment was conducted over the same area like the 2016 flights using the camera system again. Now all four sensors worked as they should (Fig. 6). To catch as many objects as possible the flight altitude was increased to 2,500 m ASL reducing the GSD by factor 3 compared to the 820 m ASL altitude in the first experiment.

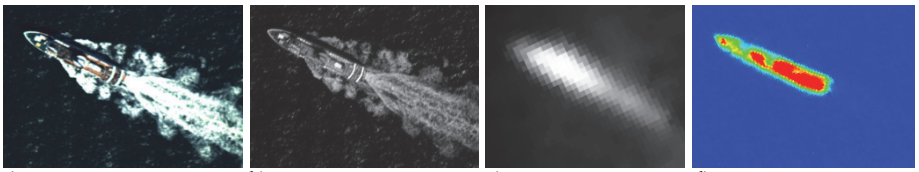

a) b) c) d)

Fig. 6. Same scene on all sensors: a) RGB 37 cm GSD, b) NIR 49 cm, c) Hyperspectral@570nm 12.20 m, d) TIR 1.22 m

4 Results

During the 2016 five days experiment approx. 12 GB of image data were radio-transmitted reliably in full geometric and radiometric resolution at a distance up to 50 km. Remote control worked stable at a distance more than 80 km.

Visual identification of ships has been investigated during low light flights. The ship names were not identifiable in the images due to near vertical perspectives. Position, heading, shape and extend were determined within a single image. Dynamic parameters like course and speed were measured by including adjacent images or images of a later fly-over. In the realtime map the ship's length was repeatedly determined between 65.7 and 66.1 m while the ship's actual length is 65.9 m. This results in a deviation of 20 cm resp. 1.5 pixels.

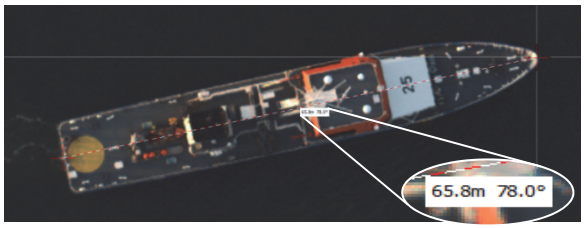

Fig. 7. Coast guard ship BP25 at solar altitude 5.5 degree (cutout)

Image-based detected occurrences (without thermal IR) were indicated real-time on the maritime management system and corresponding images were displayed.

Despite of acquiring more than 9 hours data recording no real water pollution could be observed. The popcorn was originally used to evaluate drift forecast. On the other hand the spectral signature is untypical for water pollution. Due to the high visibility in RGB and NIR imagery the popcorn was automatically extracted as an object.

The 2017 campaign added the missing thermal imagery to the data set. Object detection algorithm was activated to process this data source.

During the 2016 campaign 77 objects were observed without thermal IR Images. Due to the missing thermal IR images the object extraction on the high resolution RGB and NIR images was carried out without an object size limit of 1.5 m x 2.5 m. 73 objects were extracted correctly and four objects were not extracted.

The completeness of the automatic object extraction algorithm was 95 percent. The four missing ships were not extracted because of the object extraction size threshold. The minimum size for object detection was 25 m². Because of the missing thermal IR images a smaller object size was not applicable. Too much sun glint resulted in false positiveswhen the object size was smaller than 25 m².

Automatic object extraction extracted 65 objects false. According to this result the correctness was by 53 percent. The low correctness is explainable by the missing thermal IR information. By incorporating just RGB and NIR aerial images the backwash of the ships was very often identified as a single object (Fig. 8). The backwash of the ships was not observable in thermal IR images and increased the correctness.

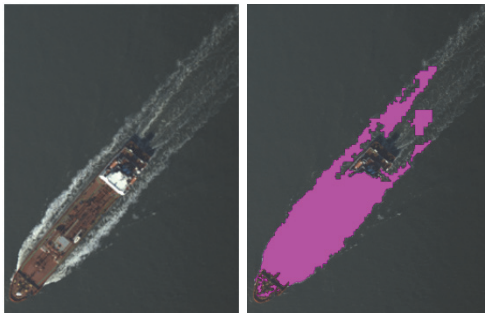

a) b)

Fig. 8. Object detection *without* thermal IR, a) original RGB image, b) multiple objects detected

Adding thermal IR images the detection quality was expected to significantly increase as shown in preliminary work [35]. The second flight campaign with thermal IR images resulted in 40 objects observed. 39 objects were correctly extracted and one object was not extracted. The acquired objects were ships and sailing boats as well as windmills (Fig. 9). The completeness of the automatic object extraction algorithm including thermal IR was 98 percent. Due to the use of this source the completeness of the automatic object detection was increased. The missing object was a small water sign.

Beside the completeness the correctness of the automatic object detection was gained. 14 objects were extracted false. According to this result the correctness raised from 53 percent to 74 percent by adding thermal IR images. All wrong extracted objects were image errors in the thermal images, which led to a peak in the according image. These peaks were detected as small objects. The results of the object detection are summarized in Table 3.

Table 3. Results of object detection

	Thermal IR images	No. of Objects	Completeness (%)	Correctness (%)
September 2016	no	77	95	53
August 2017	yes	40	98	74

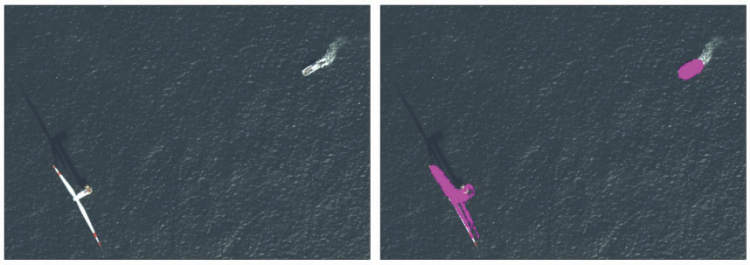

a) b)

Fig. 9. Object detection *including* thermal IR imagery, a) original RGB image, b) correctly detected objects

5 Discussion

In general the objectives of the presented sub-project – situation map and automatic object extraction – have been successfully realized and demonstrated. As shown in the results for automatic object extraction a combination of passive optical sensors is essential to achieve high rates of completeness and correctness. Because of the homogeneous water temperature and temperature differences between floating objects and surrounding water thermal IR imagery is a key information for this application. Particularly the problem of multiple detections in the RGB due to backwash can be drastically reduced by thermal IR which is directly distinguishable in the different imagery.

True-color RGB and NIR imagery are necessary to categorize objects and tag semantic information. Furthermore, high resolution RGB image data is highly beneficial for the manual interpretation by human operators. Bigger objects like ships can be characterized by measuring the size and visual interpretation. Identification of ships by name would require high resolution oblique view.

A real-time supply of object information as well as high-resolution image mosaic is a novel approach in maritime security applications. In conjunction with other information provided within the scope of the EMSec project it provides detailed information about the offshore situation in a manageable form.

6 Future Work

Next steps should be acquiring a greater database to make the algorithm more robust against image errors and thus avoiding detection of seemingly very small objects. Additionally this database can be used to feed deep learning approaches. The influence of ground pixel resolution on detection accuracy has to be examined because realtime processing on a satellite cannot be feeded with high resolution imagery as given here. By sensor data fusion the results should be improved further which will be evaluated in near future.

ACKNOWLEDGMENTS

This work was funded by the Federal Ministry of Research and Education (FKZ 13N12746). The research was supported by the Program Coordination Defence & Security Research at DLR.

References

[1] Jha, M. N., Levy, J., Gao, Y.: Advances in Remote Sensing for Oil Spill Disaster Management: State-of-the-Art Sensors Technology for Oil Spill Surveillance. Sensors 8(1), 236-255 (2008). DOI: 10.3390/s8010236

[2] Zimmermann, G., Badaev, W. W., Malkevich, M. S., Piesik, B.: The MKS-M remote-sensing experiment for determination of ocean and atmospheric parameters from SALYUT-7. Acta Astronautica 12(7-8), 475-483 (1985). DOI: https://doi.org/10.1016/0094-5765(85)90118-3

[3] Keith, D. J., Schaeffer, B. A., Lunetta, R. S., Gould Jr., R. W., Rocha, K., Cobb, D. J.: Remote sensing of selected water-quality indicators with the hyperspectral imager for the coastal ocean (HICO) sensor. International Journal of Remote Sensing 35(9), 2927–2962 (2014). DOI: http://dx.doi.org/10.1080/01431161.2014.894663

[4] Sobrino, J.A., Jiménez-Muñoz, J. C., Zarco-Tejada, P. J., Sepulcre-Cantó G., de Miguel E., Sòria, G., Romaguera, M., Julien, Y., Cuenca, J., Hidalgo, V., Franch, B., Mattar C., Morales, Gillespie, L., A., Sabol, D., Balick, L., Su, Z., Jia, L., Gieske, A., Timmermans, W., Olioso A., Nerry, F. 0, Guanter, L., Moreno, J., Shen, Q.: Thermal remote sensing from Airborne Hyperspectral Scanner data in the framework of the SPARC and SEN2FLEX projects: an overview. Hydrology and Earth System Sciences 13(11), 2031-2037 (2009). DOI: https://doi.org/10.5194/hess-13-2031-2009

[5] Legeckis, R.: A survey of worldwide sea surface temperature fronts detected by environmental satellites. Journal of Geophysical Research, 83(C9), 4501–4522 (1978). DOI: 10.1029/JC083iC09p04501

[6] Corbane, Ch., Najman, L., Pecoul, E., Demagistri, L., Petit, M.: A complete processing chain for ship detection using optical satellite imagery. International Journal of Remote Sensing 31(22), 5837-5854 (2010). DOI: 10.1080/01431161.2010.512310

[7] Müller, R., Berg, M., Casey, S., Ellis, G., Flingelli, C., Kiefl, R., Kornhoff, A., Lechner, K., Reize, T., Máttyus, G. S., Schwarz E., Simon, E., Twele, A.: Optical satellite service for EMSA (OPSSERVE)– near real-time detection of vessels and activities with optical satellite imagery. In: ESA Living Planet Symposium, pp. 2-12, ESA, Edinburgh (2012).

[8] Barrick, D.: Remote sensing of sea state by radar. In: Ocean 72 - IEEE International Conference on Engineering in the Ocean Environment, pp. 186-192, Newport, (1972). DOI: 10.1109/OCEANS.1972.1161190

[9] Daedelow, H., Schwarz, E., Voinov, S. (2016) *Near Real Time Applications to retrieve Wind Products for Maritime Situational Awareness.* DLRK 2016, 13.-15. September 2016, Braunschweig.

[10] Pavlakis, P., Sieber, A., Alexandry, S.: Monitoring oil-spill pollution in the Mediterranean with ERS SAR. ESA Earth Observation Quarterly 52, (1996).

[11] Eldhuset, K.: An automatic ship and ship wake detection system for spaceborne SAR images in coastal regions.. IEEE Transactions on Geoscience and Remote Sensing 34(4), 1010-1019 (1996). DOI: 10.1109/36.508418

[12] Brusch, S., Lehner, S.: Near real time ship detection experiments. In: Proceedings of SeaSAR, pp. 1-5. Frascati/Rome, (2010)

[13] Høye, G. K., Eriksen, T., Meland, B. J., & Narheim, B. T.: Space-based AIS for global maritime traffic monitoring. Acta Astronautica 62(2-3), 240–245 (2008). DOI: https://doi.org/10.1016/j.actaastro.2007.07.001

[14] Clazzer, F., Lázaro Blasco, F., Plass, S.: Enhanced AIS Receiver Design for Satellite Reception. CEAS Space Journal 8(4), pp. 257-268 (2016). DOI: 10.1007/s12567-016-0122-8

[15] Robbe, N., Hengstermann, T.: Remote sensing of marine oil spills from airborne platforms using multi-sensor systems. In: Water Pollution VIII: Modelling, Monitoring and Management, 347–355 (2006). DOI: 10.2495/WP060351

[16] Optimare Systems GmbH, Octopod - The All-in-One Airborne Surveillance Pod, Product Flyer, http://www.optimare.de/cms/fileadmin/PDF/GB_FEK/Flyer-DINA3-OctoPod-28-02-2017-ENGL_klein.pdf, last accessed 2017/10/12.

[17] Fischer, Y, Bauer, A.: Object-oriented sensor data fusion for wide maritime surveillance. In: International WaterSide Security Conference, Carrara, 2010, pp. 1-6 (2010). DOI: 10.1109/WSSC.2010.5730244

[18] Gruener, K.: The Three-Frequency Microwave Radiometer of a 2nd Generation Airborne Surveillance System for Remote Sensing of Maritime Oil Pollution. In: Proceedings of IEEE Workshop RF and Microwave Noise, pp. 66-69 . Ilmenau (1996).

[19] L3-WESCAM, MX-25 Technical Data Sheet, http://www.wescam.com/wp-content/uploads/PDS-MX-25-25D-January-2017.pdf, last accessed 2017/10/12.

[20] The Maritime Safety and Security Center, http://www.msz-cuxhaven.de/EN/Home/home_node.html, last accessed 2017/10/12.

[21] European Maritime Safety Agency, Annual Overview of Marine Casualties and Incidents, http://www.emsa.europa.eu/news-a-press-centre/external-news/item/2903-annual-overview-of-marine-casualties-and-incidents-2016.html, last accessed 2017/10/12.

[22] Kay, S., Hedley, J. D., Lavender, S.: Sun Glint Correction of High and Low Spatial Resolution Images of Aquatic Scenes: a Review of Methods for Visible and Near-Infrared Wavelengths. Remote Sensing 1(4), 697-730 (2009). DOI: 10.3390/rs1040697

[23] Streher, A. S., Goodman, J. A., Soares Galvao, L. , Faria Barbosa, C. C., Freire Silva, T. S., Leao de Moraes Novo, E. M.: Sunglint temoval in high spatial resolution hyperspectral images under different viewing geometries. In: Anais XVI Simpósio Brasileiro de Sensoriamento Remoto, pp. 7958-7965. Brasil (2013).

[24] Gholizadeh, M. H., Melesse, A. M., Reddi, L. (2016): A Comprehensive Review on Water Quality Parameters Estimation Using Remote Sensing Techniques. Sensors (Basel, Switzerland), 16(8), 1298. http://doi.org/10.3390/s16081298

[25] Krawczyk, H., Neumann, A., Riha, S.: Multivariate interpretation algorithm for water quality in the Baltic Sea. In: Proceedings of SPIE 7473, Remote Sensing of the Ocean, Sea Ice, and Large Water Regions 7473, Berlin. DOI: 10.1117/12.830400

[26] Dougherty, E.: Introduction to Morphological Image Processing, SPIE Press, Michigan, 1992.

[27] Egenhofer M. J.: A Model for Detailed Binary Topological Relationships. Geomatica 47(3&4), pp. 261-273 (1993). DOI: doi=10.1.1.16.2075

[28] Winter, S.: Beobachtungsunsicherheit und topologische Relationen. In: Workshop Datenqualität und Metainformation in Geo-Informationssystemen, pp. 141-154. Rostock (1996).

[29] Straub, B.-M.: Automatische Extraktion von Bäumen aus Fernerkundungsdaten. Hannover (2003).

[30] Lehmann, F., Berger, R., Brauchle, J., Hein, D., Meißner, H. Pless, S., Strackenbrock, B., Wieden, A.: MACS – Modular airborne camera system for generating photogrammetric high-resolution products. In: Deutsche Gesellschaft für Geowissenschaften, 6, pp. 435–446 (2011). DOI: 10.1127/1432-8364/2011/0096

[31] Brauchle, J., Hein, D., Berger, R.,: Detailed and highly accurate 3D models of high mountain areas by the MACS-Himalaya aerial camera platform, in: Int. Arch. Photogramm. Remote Sens. Spatial Inf. Sci., XL-7/W3, 1129–1 (2015). DOI: 10.5194/isprsarchives-XL-7-W3-1129-2015

[32] Wieden, A., Stebner, K.,: Referenzorientierung für Bilddaten aus Mehrkopfkamerasystemen. In: DGPF Tagungsband 22, pp. 518–525 (2013).

[33] Suhr, B., Lange, A-Th., Mohrs, R.: Automatische Detektion von AIS Auffälligkeiten in naher Echtzeit. In. Deutscher Luft- und Raumfahrtkongress (DLRK). Braunschweig (2016).

[34] Kreienfeld, M., Giese, K.: Development of a RPV- Demonstrator for Maritime Security Applications. In: Deutscher Luft- und Raumfahrt Kongress. Rostock (2015)

[35] Scherbaum, P., Brauchle, J., Kraft, Th., Pless, S.: MACS-Mar – A Real-Time Capable Multisensor Remote Sensing System for Maritime Applications. In: IEEE International Conference on Aerospace Electronics and Remote Sensing Technology (ICARES). Curan Associates, Inc. ICARES, Kuta, Bali, Indonesien (2015). DOI: 10.1109/ICARES.2015.7429839